Acta Geologica Sinica (English Edition), 2020, 94(1): 27–37

A Floating Astronomical Time Scale for the Early Late Cretaceous Continental Strata in the Songliao Basin, Northeastern China

MA Xiaojuan[1, 2], WU Huaichun[1, 2, *], FANG Qiang[1, 2], SHI Meinan[1, 2], ZHANG Shihong[1], YANG Tianshui[1], LI Haiyan[1] and WANG Chengshan[1]

[1] *Schoolof Ocean Sciences, China University of Geosciences, Beijing 100083, China*
[2] *State Key Laboratory of Biogeology and Environmental Geology, China University of Geosciences, Beijing 100083, China*

Abstract: A continuous terrestrial succession was recovered from the Songke-2 (SK-2) borehole in the Songliao Basin, Northeastern China. This borehole provides a unique material for further research on the continental paleoclimate during Cretaceous greenhouse period, following a series of achievements of the Songke-1 (SK-1) core. In this study, thorium (Th) logging data were chosen as a paleoclimate proxy to conduct a detailed cyclostratigraphic analysis. The Th series varies quasi-periodically; power spectra and evolutionary fast Fourier transformation (FFT) analysis reveal significant cycles in the Quantou (K_2q), Qingshankou (K_2qn), Yaojia (K_2y) and Nenjiang (K_2n) formations. The ratio of cycle wavelengths in these stratigraphic units is approximately 20:5:2:1, corresponding to long orbital eccentricity (405 kyr), short orbital eccentricity (100 kyr), obliquity (37 kyr), and precession cycles (22.5 kyr and 18.4 kyr). The durations of the K_2n, K_2y, K_2qn and K_2q are estimated as 6.97, 1.83, 5.30 and 4.52 Myr, respectively, based on the constructed ~18.62 Myr "floating" astronomical time scale (ATS). Comparison of the durations between the SK-1s and SK-2 boreholes exhibits a slight difference of 0.06 Myr and 0.459 Myr for K_2qn and K_2y. Nevertheless, our ATS of K_2n supports the chronostratigraphic frame constructed by the CA-ID-TIMS data of the SK-1s borehole. This new "floating" ATS provides precise numerical ages for stratigraphic boundaries, biozones and geological events in the Songliao Basin, and can serve as a basis for correlation of strata and events between marine and terrestrial systems.

Key words: Late Cretaceous, SK-2 borehole, cyclostratigraphy, astronomical time scale, Songliao Basin, northeastern China

Citation: Ma et al., 2020. A Floating Astronomical Time Scale for the Early Late Cretaceous Continental Strata in the Songliao Basin, Northeastern China. Acta Geologica Sinica (English Edition), 94(1): 27–37. DOI: 10.1111/1755-6724.14497

1 Introduction

The Cretaceous Period experienced typical greenhouse conditions. During this time, multiple geological events occurred, including oceanic anoxic events (OAEs), widespread volcanic activities and oceanic red beds. Marine geological archives from the Umbria–Marche Basin (Fiet et al., 2001; Grippo, 2003), Western Interior Basin (Locklair and Segeman, 2008; Meyers et al., 2012; Ma et al., 2014) and Ocean Drilling Program (ODP) and International Ocean Discovery Program (IODP) cores (Husson et al., 2011) etc. have greatly contributed to the understanding of these events by the virtue of their continuous records. As an essential part of the Earth system, records from the terrestrial domain should be studied to elucidate its response to both regional and global paleoclimate (e.g., Olsen and Kent, 1996, 1999; Wang et al., 2013a).

As one of the largest Cretaceous terrestrial basins in the world, the Songliao Basin offers us a unique opportunity to decipher the terrestrial response to the climate changes because of its nearly complete record of Upper Cretaceous lacustrine strata. The SK-1 Scientific Drilling Project, including the SK-1 south (SK-1s) and north (SK-1n) boreholes, was accomplished and the integrated chronostratigraphic framework for the drill cores has been established. Zhao et al. (2013) and Wan et al. (2013) had established the multi-disiplinary sporopollen and dinoflagellate biostratigraphic schemes. In addition, four SIMS zircon U–Pb ages and a complete geomagnetic polarity chronsequence from upper C34n to C29n was constructed to establish a temporal framework (He et al., 2012; Deng et al., 2013). An ~27 Myr astronomical time scale (ATS) was constructed to refine the geochronology for the SK-1 boreholes after tuning the extracted 405 kyr-eccentricity cycles to the astronomical target curve (Wu et al., 2013, 2014). The temporal framework for the lower Turonian–lower Campanian of the SK-1 boreholes is still under debate. The sediment accumulation rate (SAR) indicated by four new CA-ID-TIMS U–Pb ages (Wang et al., 2016) yields a more uniform average SAR than that calculated from the ATS (Wu et al., 2013); thus, further investigation of this issue is required.

In this paper, we conducted a cyclostratigraphic

* Corresponding author. E-mail: whcgeo@cugb.edu.cn

research on the high-resolution thorium (Th) logging data from the Nenjiang Formation (K_2n), Yaojia Formation (K_2y), Qingshankou Formation (K_2qn) and Quantou Formation (K_2q) in the International Continental Scientific Drilling Program (ICDP) SK-2 borehole in order to reveal the astronomical signals in the sedimentary records. The scientific objectives are to establish a "floating" ATS based on the bandpass filtered 405-kyr long eccentricity cycles in these sedimentary records, and to conduct a primary correlation with the chronostratigraphic framework for the SK-1s core.

2 Geological Setting and the SK-2 Borehole

2.1 Geological setting

The Songliao Basin, the longest-lived supersized terrestrial basin of the Cretaceous Period, is located between 119°40′–128°24′E and 42°25′–49°23′N in Heilongjiang, Jilin and Liaoning provinces of northeastern China (Fig. 1a). The basin is 700 km long from north to south, and 370 km wide from east to west, covering an area of approximately 260,000 km^2. The basin trends in a NNE direction and is geographically surrounded by the Great Xing'an Range in the west, the Lesser Xing'an Range in the north and the Zhangguangcai Range in the east (Wu et al., 2001). The evolution of the Songliao Basin took place in four stages (pre-rift doming, synrift, post-rift thermal subsidence and structural inversion) from the pre-Late Jurassic to Latest Cretaceous (Wang et al., 2007; Feng et al., 2010; Wang et al., 2013b).

The basement of the Songliao Basin consists of Precambrian to Paleozoic metamorphic and igneous rocks

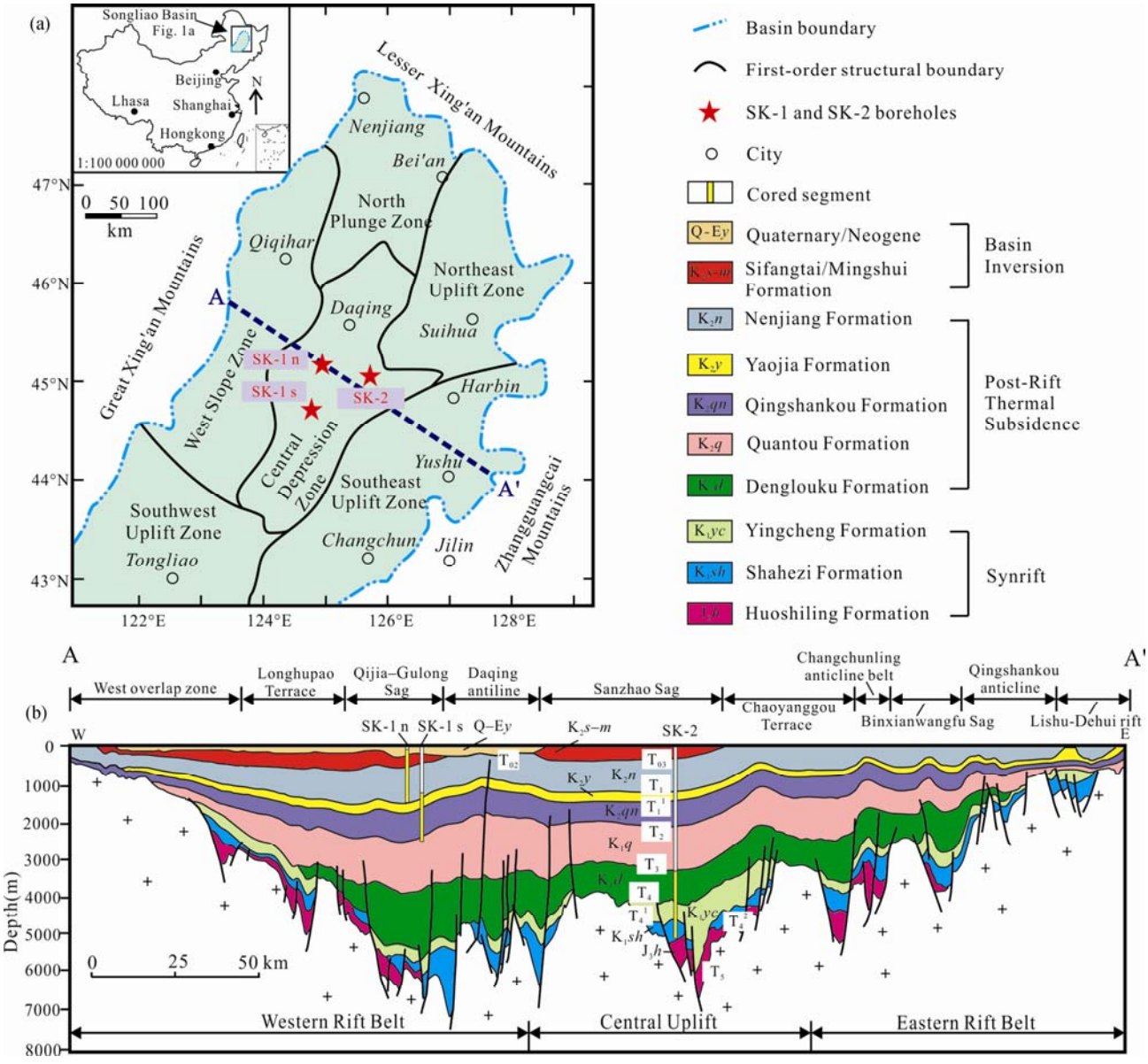

Fig. 1. (a) Schematic map of the Songliao Basin showing distribution of first-order tectonic units and location of the SK-1s, SK-1n and SK-2 boreholes (modified from Feng et al., 2010). (b) Structural cross section (A–A′) across the central part of the Songliao Basin based on regional seismic analysis (modified from Feng et al., 2010; Wang et al., 2013b).
The yellow bars in SK-1n, SK-1s, and SK-2 are cored intervals and the white bars are un-cored intervals.

and Paleozoic to Mesozoic granites (Wu et al., 2001). Overlying the basement, the Mesozoic–Cenozoic terrestrial strata, consisting of up to 7 km thickness of volcanic, volcaniclastic, alluvial-fan, fluvial and lacustrine sediments, are evenly distributed across the basin (Gao et al., 1994).The Upper Jurassic and Cretaceous strata in the basin can be divided into ten lithologic formations (Fig. 1b), which are from oldest to youngest the Huoshiling (J_3h), Shahezi (K_1s), Yingcheng (K_1y), Denglouku (K_1d), Quantou (K_2q), Qingshankou (K_2qn), Yaojia (K_2y), Nenjiang (K_2n), Sifangtai (K_2s) and Mingshui (K_2m) formations (Sha et al., 2007; Wang et al., 2007; Feng et al., 2010).

The paleoclimate of the Songliao Basin during the Cretaceous has been extensively discussed on the basis of sporopollen assemblages (Huang et al., 1999; Zhao, 2013) and oxygen isotopic data (Chamberlain et al., 2013; Gao et al., 2015), with the conclusion that the basin was mainly experienced a humid to semihumid warm temperate–subtropical climate during this period (Wang et al., 2013b). In addition, Huang et al. (1999) and Zhao (2013) stated that in these warm conditions small apparent saltations in temperature and humidity still occurred.

2.2 The SK-2 borehole

The SK-2 borehole is located at the central depression zone of the Songliao Basin (Fig. 1). The drilling project was started in 2014 and completed with a total drilling depth of 7018 m in March of 2018, and the SK-2 borehole is considered as the deepest continental scientific exploratory well in the ICDP history. It was drilled through the whole Cretaceous strata. Continuously coring began at the bottom of the Denglouku Formation (K_1d; 2865 m), with a total core length of 4134.81 m and a recovery ratio of 96.61% (Zhu et al., 2018). The stratigraphic units in SK-2 include, from youngest to oldest, the Upper Cretaceous Mingshui Formation (K_2m), Sifangtai Formation (K_2s), Nenjiang Formation (K_2n), Yaojia Formation (K_2y), Qingshankou Formation (K_2qn) and Quantou Formation (K_2q); the Lower Cretaceous Denglouku Formation (K_1d), Yingcheng Formation (K_1y), and Shahezi Formation (K_1s); and the Upper Jurassic Huoshiling Formation (J_3h; Fig. 1).

In this study, we mainly focused on the sedimentary cycles recorded in the early Upper Cretaceous Nenjiang (K_2n), Yaojia (K_2y), Qingshankou (K_2qn) and Quantou (K_2q) formations. The Nenjiang Formation (435.125–1250.5 m) is divided into five members. Members 1 and 2 (K_2n^{1+2}) are dominated by dark gray to black mudstone interbedded with oil shale (Fig. 2). K_2n^{1+2} was deposited in deep-water lacustrine facies, representing an important period of large-scale lake expansion after the deposition of the Qingshankou Formation (Feng et al., 2010). Members 3 and 4 comprise gray mudstone, siltstone, muddy siltstone and silty mudstone of fluvial, shallow-lacustrine and deltaic origins, and K_2n^5 is characterized by gray-green, purple-red and gray to black mudstone, silty mudstone and siltstone (Fig. 2). During the deposition of members 3–5 (K_2n^{3-5}), the lowering of the lake level was associated with a hotter and dryer climate.

The Yaojia Formation (1250.5–1371 m) comprises gray, grayish-green and black mudstone, siltstone, muddy siltstone and silty mudstone, with purple-red mudstone at the bottom (Fig. 3). The lake level in K_2y^1 and K_2qn^{2+3} deposition period has maintained stable and rose in K_2y^{2+3} time. The main depositional facies in this period were fluvial and deltaic facies (Feng et al., 2010; Gao, 2015).

The Qingshankou Formation (1371–1676.5 m) is composed of grayish, dark gray and black mudstone, interbedded with oil shale in the lower part and thin-bedded grayish siltstone and muddy siltstone in the upper part (Fig. 3). The lake level reached its maximum during early Qingshankou deposition time and tended to fall in K_2qn^{2+3}; in addition, the depositional environment changed from deep lacustrine facies to shallow lake and delta (Feng et al., 2010; Gao, 2015).

The Quantou Formation (1676.5–2535.5 m) is divided into four members. Members 1–3 are mainly characterized by red-brown, purple-red mudstone and silty mudstone interbedded with thin grayish siltstone and muddy siltstone; member 4 consists of thicker purple-red or black mudstone, gray-green silty mudstone and grayish siltstone (Fig. 4). The depositional environment changed from meandering river and floodplain in members 1–2 (K_2q^{1+2}) to delta front and shallow lake in members 3–4 (K_2q^{3+4}; Feng et al., 2010).

3 Data and Method

3.1 Thorium (Th) logging data

Natural gamma-ray (GR) logging data, which are dominated by the amounts of the radioactive atomic nuclei of potassium (K), uranium (U) and thorium (Th), can be used in paleoclimatic and paleoenvironmental researches (Schnyder et al., 2006). Th is concentrated in some of the sedimentary host minerals such as clays and feldspar. According to Schnyder et al. (2006), Th is more likely to be preserved and partially concentrated during weathering because it is more insoluble than K and U. The Th logging data of the SK-2 borehole exhibit regular variations as the lithology changes, with high Th levels in mudstones and low Th concentrations in sandstones (Figs. 2–4). From the cyclostratigraphic analysis of the SK-1s borehole, astronomical forcing had a strong impact on the climate and environment of the Songliao Basin during the Late Cretaceous (Wu et al., 2013). During periods of high eccentricity, the hotter and wetter climate would have resulted in intensified weathering and monsoon, as well as enhancing the inputs of clay mineral and nutrient materials, resulting in higher productivity in the paleolake (Wu et al., 2013). Thus, higher Th valu eindicates a higher clay content in the sediment during higher eccentricity period. Accordingly, we choose the Th logging data as a paleoclimatic proxy for cyclostratigraphic analysis in this study.

3.2 Time series methods

The Th logging series were divided into five subsets and analyzed separately (see below).

The Th logging series of five subsets were respectively linearly interpolated to a uniform spacing of 0.5 m in Subsets 1 and 5, and 0.3 m in Subsets 2, 3 and 4 (Figs. 2–

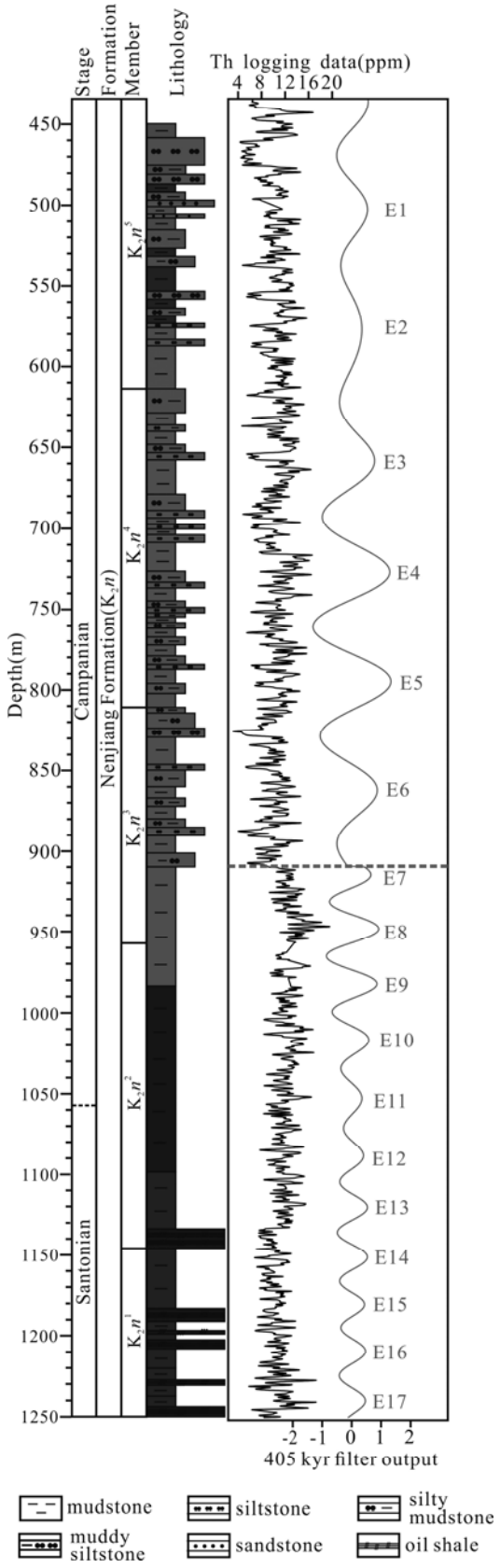

Fig. 2. Lithology, Th logging data and cyclostratigraphy for the Nenjiang Formation (K^2n; Subset 1 and Subset 2) of the SK-2 borehole.

The interpreted 405-kyr cycle was extracted with Gauss filters with passbands of 0.0145 ± 0.002 cycles/m (Subset 1, 435.125 – 910 m) and 0.0305 ± 0.0025 cycles/m (Subset 2, 910 – 1250.5 m), respectively. The dashed line on the right part shows the boundary of Subset 1 and Subset 2. The "E" represents the 405-kyr long eccentricity cycle. The stage boundaries are from Wang et al. (2013b).

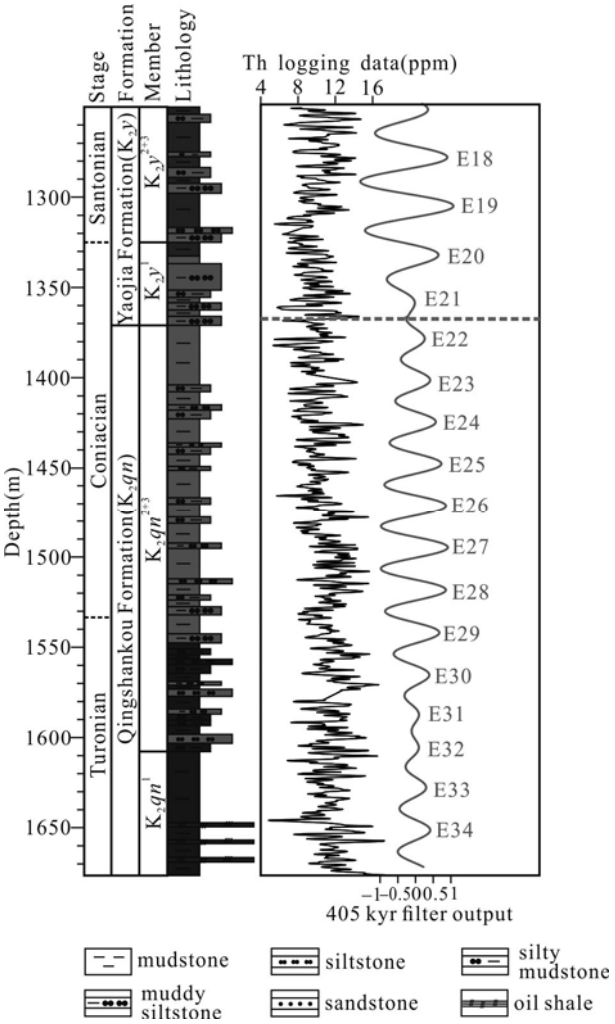

Fig. 3. Lithology, Th logging data and cyclostratigraphy for the Yaojia (K_2y; Subset 3) and Qingshankou (K_2qn; Subset 4) formations of the SK-2 borehole.

The interpreted 405-kyr cycle was extracted with Gauss filters with passbands of 0.036± 0.01 cycles/m (Subset 3, 1250.5–1371 m) and 0.0415 ± 0.0065 cycles/m (Subset 4, 1371–1676.5 m). The dashed line on the right part shows the boundary of Subset 3 and Subset 4. The "E" represents the 405-kyr long eccentricity cycle. The stage boundaries are from Wang et al. (2013b).

4). These subsets were detrended by smoothing in Matlab. Spectral analysis of the unturned Th logging series was performed using the multitaper method (MTM; Thomson, 1982) with classical red noise modeling reported at the 50%, 90%, 95%, and 99% confidence levels (CLs) with Matlab scripts available at (http://mason.gmu.edu/~lhinnov/cyclostratigraphytools.html). Evolutionary fast Fourier transform analysis (FFT; Kodama and Hinnov, 2015) was conducted to identify the changes in spatial cycle frequencies throughout the record. The correlation

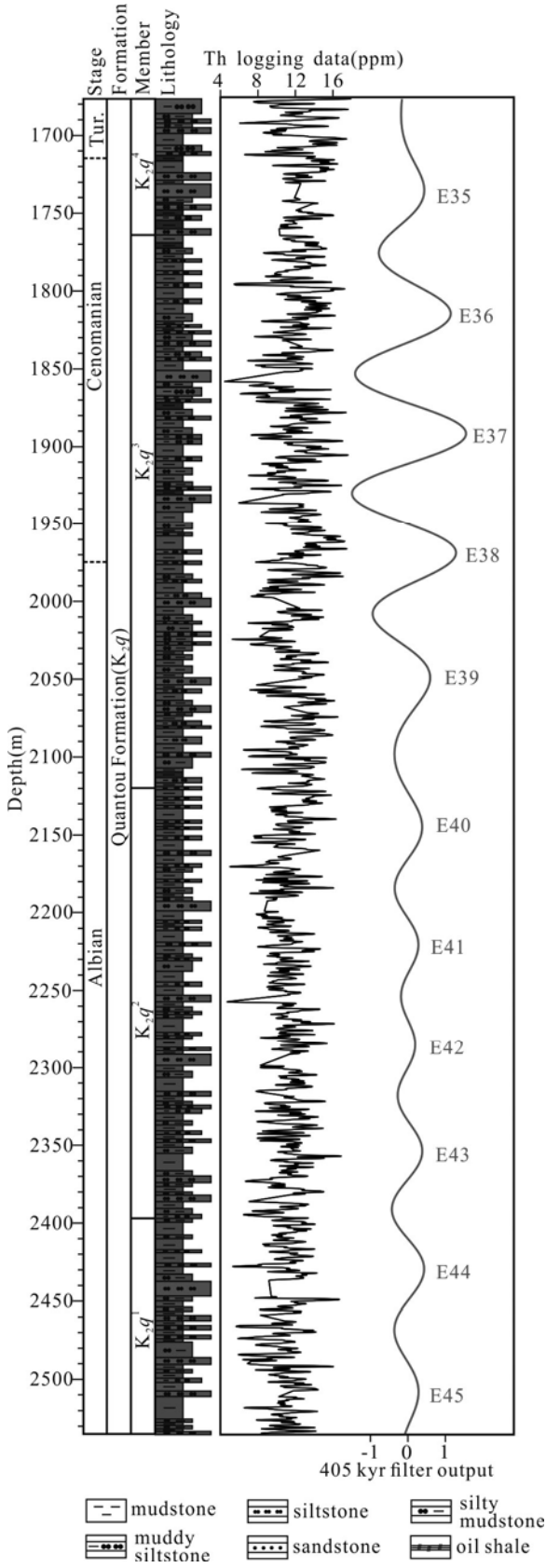

Fig. 4. Lithology, Th logging data and cyclostratigraphy for the Quantou (K_2q) Formation (Subset 5) of the SK-2 borehole.

The interpreted 405-kyr was extracted with Gauss filters with passbands of 0.013 ± 0.004 cycles/m (Subset 5, 1676.5 – 2535.5 m). The "E" represents the 405 -kyr long eccentricity cycle. The stage boundaries are from Wang et al. (2013b).

coefficient (COCO; Li et al., 2018) procedures in ACycle v2.0.6 were additionally applied to confirm the presence of astronomical signals and assess the optimal SAR in the Th logging series. Gaussian bandpass filtering was carried out to extract the interpreted 405-kyr eccentricity sedimentary cycle using bandpass routine of the Astrochron package (Meyers, 2014) in R. Finally, the Th logging series was converted from the stratigraphic to time domain in Matlab via *depthtotime.m* script (Kodama and Hinnov, 2015).

Both La2004 and La2010 astronomical solutions considered the 405-kyr eccentricity term to be stable and accurate during the Cretaceous Period (Laskar et al., 2004, 2011). Consulting the MTM spectra of ETP signal of the La2004 and La2010a solutions with the interval of 83–93 Ma by Wu et al. (2013), we here use a Late Cretaceous astronomical target of 405 kyr (long eccentricity), 131 kyr and 99 kyr (short eccentricity), 37 kyr (obliquity), and 22.5 kyr and 18.3 kyr (presession).

4 Results and Discussion

4.1 Cyclostratigraphic analysis

4.1.1 Spectral analysis

The Th values range from 3.13 to 19.61 ppm and show clear cyclic patterns (Figs. 2–4). Because of the dramatic changes in sedimentary environments, the lithology and SAR throughout the section are not constant. The depositional facies of K_2n changed from deep-water lacustrine in K_2n^{1+2} to fluvial, shallow lacustrine and delta in K_2n^{3-5}, at the depth ~910 m. K_2qn to K_2y were deposited as the lake gradually shrank. The main lithologies of these two formations are mudstone, siltstone, muddy siltstone and silty mudstone, which were deposited as the sedimentary environments changed from deep lacustrine (K_2qn^1) to shallow lake (K_2qn^{2+3}), fluvial and delta (K_2y). Throughout the K_2q, the frequent changes in lake level resulted in interbedding of mudstone and thinner siltstone. In addition, inspection of the evolutionary FFT spectrogram also reveals two major shifts in frequency close to 910 m (where the lithology begins to change in K_2n^3) and 1676.5 m (the K_2qn/K_2q boundary). As shown in Fig. 5a, the low-frequency components continuously shift towards higher frequencies in the intervals 910–1250.5 m, 1250.5–1371 m and 1371–1676.5 m intervals, and exhibit a reverse shift at 1676.5–2535.5 m, indicating distinct decreased sedimentation rates at 910–1250.5 m 1250.5–1371 m and 1371–1676.5 m. Thus, five stratigraphic subsets for the depth intervals of 435.125–910 m (Subset 1; K_2n^5, K_2n^4, and upper K_2n^3), 910–1250.5 m (Subset 2; lower K_2n^3, K_2n^2 and K_2n^1), 1250.5–1371 m (Subset 3; K_2y), 1371–1676.5 m (Subset 4; K_2qn) and 1676.5–2535.5 m (Subset 5; K_2q) were defined for the Th logging data, and 2π MTM spectral analyses were conducted for each subset (Fig. 5b–f). In addition, with the hypothesis of a constant SAR for each subset, COCO analysis was performed to inspect the impact that astronomical forcing has on proxy records and to obtain the optimal sedimentation rates (Fig. 6). The Monte Carlo simulation approach was used to obtain a null hypothesis significance level (H_0-SL), of which a

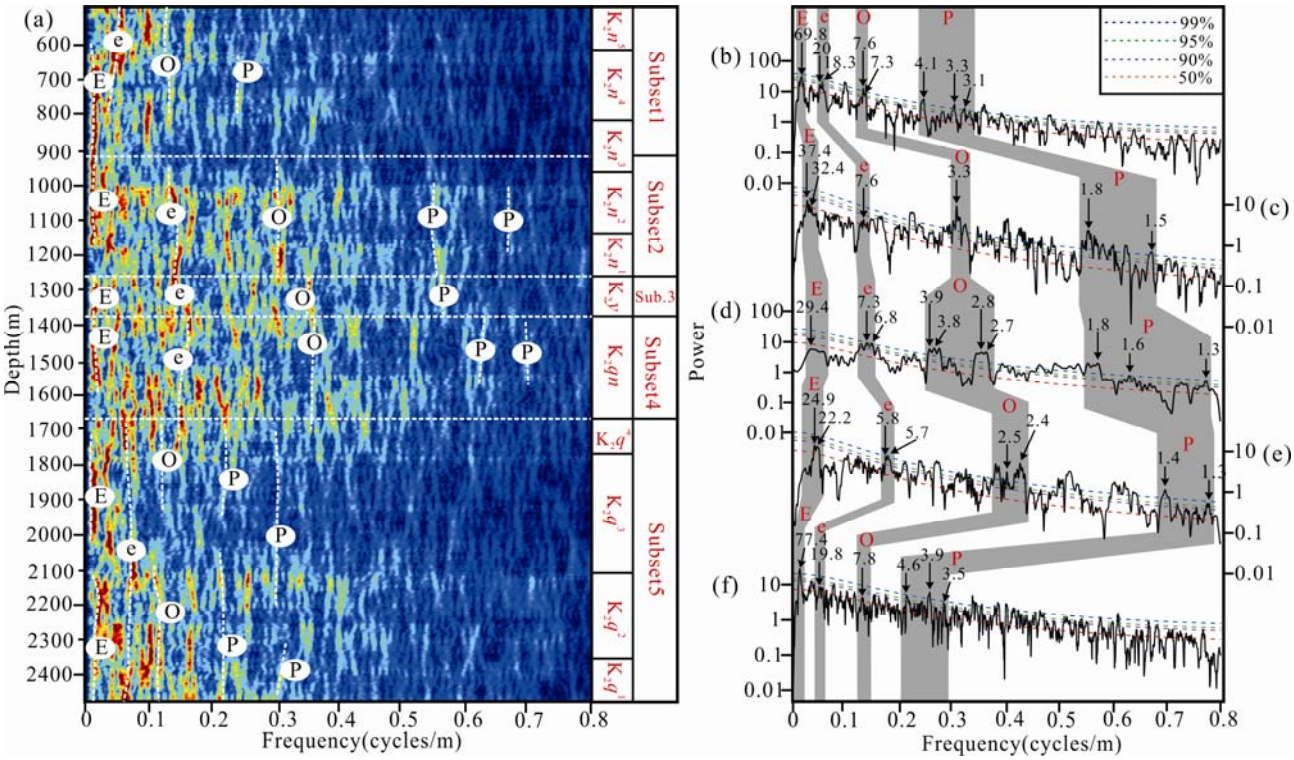

Fig. 5. (a) Evolutionary fast Fourier transform spectrum of the untuned Th series of the SK-2 borehole, with a sliding window of 120 m and depth interval of 435.125–2535.5 m. 2π MTM power spectrum of the unturned Th series of Subset 1 (b), Subset 2 (c), Subset 3 (d), Subset 4 (e) and Subset 5 (f).

Significant peaks are labeled in meters. E, e, O and P represent the long eccentricity, short eccentricity, obliquity and precession cycles, respectively. White horizontal lines (dashed) in (a) indicate the boundaries between the adjacent subsets. The red, purple, green and blue (dashed) curves represent the 50%, 90%, 95% and 99% CLs. Sub.3 represents Subset 3.

lower value represents a better match between the stratigraphic frequencies and orbital frequencies.

The 2π MTM power spectrum of the untuned Th series of Subset 1 reveals significant cycles with wavelengths of 69.8, 20 and 18.3 m exceeding the 95% CL and 7.6, 7.3, 4.1, 3.3 and 3.1 m above the 99% CL (Fig. 5b). The wavelengths of 69.8, ~18–20, ~7–8 and ~3–4 m have a ratio comparable with the Late Cretaceous orbital parameters; thus, they are primarily interpreted as E, e, O and P cycles, respectively. COCO analysis additionally shows that the estimated correlation coefficient (ρ) reaches its maximum when SAR is focused at 14.4 and 17 cm/kyr. The null hypothesis test is lower than 1%, which means the null hypothesis of no orbital signal can be rejected at a 99% (Fig. 6a). With this interpretation, the alternative 405 -kyr eccentricity cycles would be 58.32 m and 68.85 m; the latter conforms to the 69.8-m cycles in the 2π MTM spectrum.

For Subset 2, the COCO analysis produced an optimal SAR of 8.4 cm/kyr, with an H_0-SL of 0.399% (Fig. 6b). Thus, the possibility of the 34.02-m cycle corresponding to the 405-kyr eccentricity cycle can be 99.601%, which is consistent with the 32.4–37.4-m wavelengths in the 2π MTM spectrum (Fig. 5c). Hence, the peaks with wavelengths of 7.6 m exceeding the 50% CL and 3.3, 1.8 and 1.5 m above the 99% CL in the 2π MTM power spectrum might represent the sedimentary cycles related to e, O and P forcing.

The 2π MTM power spectrum of the untuned Th series of Subset 3 reveals significant cycles with wavelengths of 7.3 and 1.3 m exceeding the 95% CL and 6.8, 3.9, 2.8, 1.8 and 1.6 m above the 99% CL (Fig. 5d). These cycles are primarily interpreted as the e, O and P cycles,, respectively. COCO analysis additionally produced an optima SAR of 7.4 cm/kyr with an H_0-SL of 3.4% (Fig. 6c); thus, the 29.9-m cycles consistent with the 29.4-m wavelengths in the 2π MTM spectrum (Fig. 5d) could represent the 405-kyr eccentricity cycle.

For Subset 4, 2000 Monte Carlo simulations of the null hypothesis test indicate that a SAR of 5.5 cm/kyr yields a significance level lower than 0.1% CL (Fig. 6d). Thus, the 22.3-m cycle which approximates to the 24.9-m and 22.2-m signals interpreted in the 2π MTM spectrum (Fig. 5e), is 99.9% likely to represent the 405-kyr eccentricity cycles. The significant peaks with wavelengths of 5.8, 2.5 and 1.4 m above the 99% CL (Fig. 5e) are primarily ascribed to the e, O and P cycles, respectively.

The COCO analysis of Subset 5 reveals a broad minimum in estimated H_0-SL (lower than 1%) with a range of SAR of 18.1–21.5 cm/kyr (Fig. 6e). Based on this result, the most possible 405-kyr eccentricity cycle was calculated to be 73.31–87.08 m, in agreement with the apparent peak with a wavelength of 77.4 m above the 99% CL in the 2π MTM spectrum (Fig. 5f). Accordingly, the

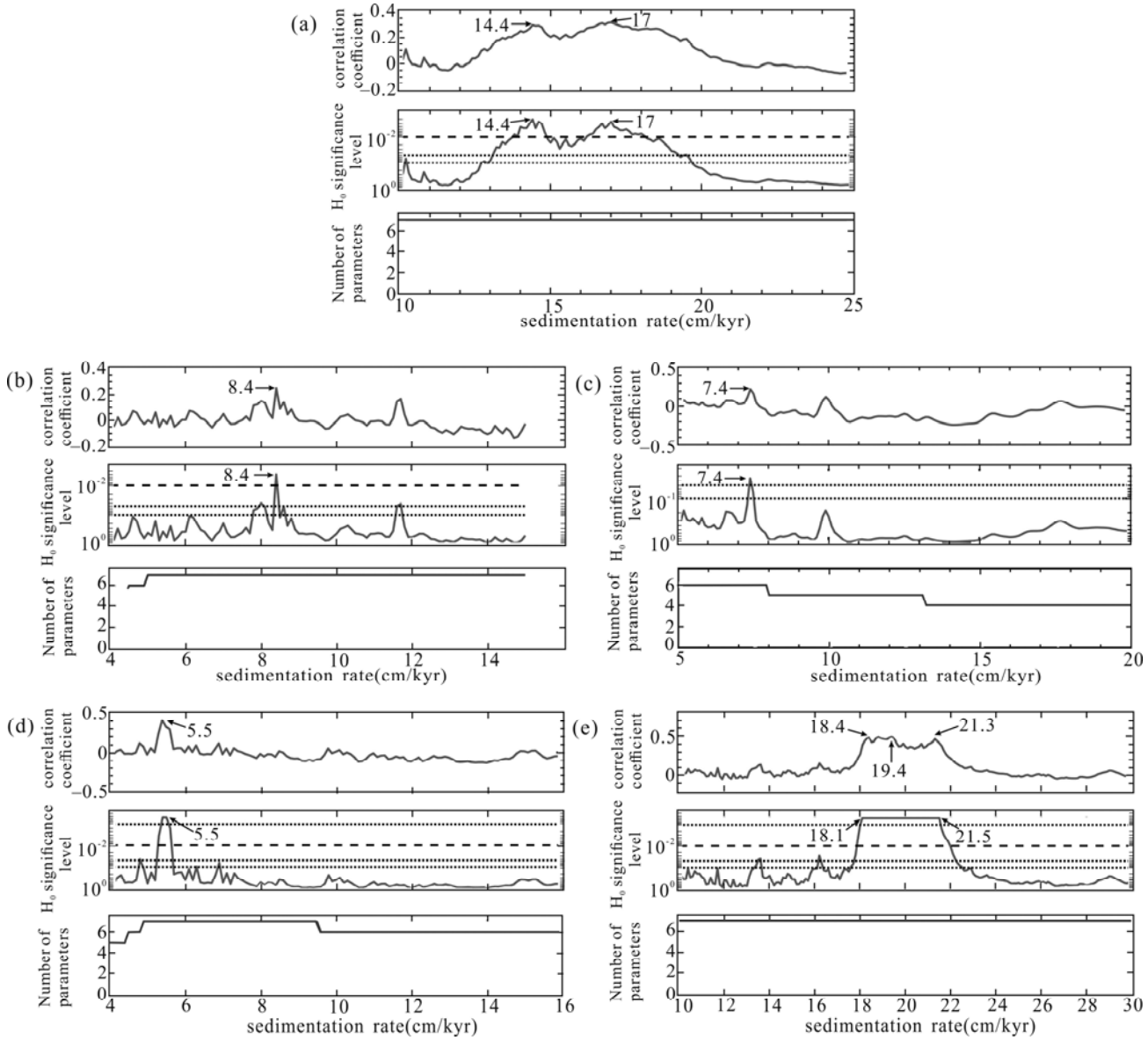

Fig. 6. COCO analyses of the unturned Th logging series of Subset 1(a), Subset 2(b), Subset 3(c), Subset 4(d) and Subset 5(e).
The parameters used for analyses are as follows: Subset 1: the sedimentation rate ranges from 10 to 25 cm/kyr and the target age is 78 Ma; Subset 2: the SAR ranges from 4 to 15 cm/kyr and the target age is 80 Ma; Subset 3: the sedimentation rate ranges from 5 to 20 cm/kyr and the target age is 86 Ma; Subset 4: the sedimentation rate ranges from 4-16 cm/kyr and target age is 89 Ma; Subset 5: the sedimentation rate ranges from 10 to 30 cm/kyr and the target age is 92 Ma. The target ages were set considering the CA-ID-TIMS U–Pb ages by Wang et al. (2016) and the ATS by Wu et al. (2013, 2014) for the SK-1 boreholes. For all of the subsets, the tested sedimentation rate step is 0.1 cm/kyr and the number of Monte Carlo simulations is 2000. From top to bottom in each panel: the correlation coefficient (ρ) spectrum; null hypothesis test, and the number of contributing astronomical frequencies.

peaks with wavelengths of 19.8, 7.8 and 3.5–4.6 m (Fig. 5f) could be interpreted as e, O and P forced sedimentary cycles, respectively.

The results of COCO analyses above, on the one hand, attest to the validity of our interpretations of the sedimentation cycles, and, on the other hand, help to reveal the SAR variations during the post-rift thermal subsidence stage of the basin evolution. The average SAR for each formation was calculated and shown in Table 1. K_2q had the highest mean SAR of 19.11 cm/kyr throughout the section, with widely developed purple-red mudstone and grayish muddy siltstone and siltstone. As the lake level rose, the mean SAR sharply decreased to 5.76 cm/kyr in K_2qn, and then increased slightly to 6.58 cm/kyr in K_2y. The SAR of K_2n tended to be more variable as a result of the relatively complex sedimentary environment. The average SAR of K_2n^{1+2} slightly rose but still maintained a low value of 8.21 cm/kyr; however, a high mean SAR of 15.35 cm/kyr happened in K_2n^{3-5}. This variation in SAR mainly results from the anomalous subsidence of the Songliao Basin during the post-rift period. According to Li et al. (2014), there are two subsidence fastigium occurred during the K_2q and K_2n periods, which well explains the high SAR of K_2q and K_2n^{3-5}. For K_2qn, K_2y and K_2n^{1+2}, the persistent low SAR is possibly caused by the great lake transgression during

Table 1 Formation depth, thicknesses, average SARs and durations for the SK-1s and SK-2 boreholes

Formation	SK-1s (Wu et al., 2013)				SK-2 (this study)			
	Depth (m)	Thickness (m)	Mean SAR (cm/kyr)	Duration (Myr)	Depth (m)	Thickness (m)	Mean SAR (cm/kyr)	Duration (Myr)
K_2n^{3-5}	/	/	/	/	435–957.5	522.5	15.35	3.403
K_2n^{1+2}	960–1128.17	168.17	13.2	1.373	957.5–1250.5	293	8.21	3.569
K_2y	1128.17–1285.91	157.74	11.8	1.337	1250.5–1371	120.5	6.58	1.832
K_2qn	1285.91–1782.93	497.02	9.27	5.361	1371–1676.5	305.5	5.76	5.301
K_2q	/	/	/	/	1676.5–2535.5	859	19.01	4.519

K_2qn^1 and K_2n^{1+2} controlled by the fluctuation of paleolake level, which could have had a non-negligible impact on the sedimentary mineral type (Huang et al., 2013; Hu et al., 2015). Furthermore, it is considered that changes in SAR have a close association with astronomically driven enhanced siliciclastic inputs during wet and warm periods, as SAR maxima corresponds to long eccentricity maxima (Wu et al., 2013, 2014).

4.1.2 Astronomical calibration

As the 405-kyr orbital eccentricity cycle is considered consistent throughout the geological time (Laskar et al., 2004), it is feasible to use this cycle for the astronomical calibration of the Th logging series. Based on the spectral interpretation above, Gaussian bandpass filters were designed to isolate the 405-kyr cycles in the stratigraphic records. As a result, ~6, ~11, ~4, ~13 and ~11 long eccentricity cycles were recognized for subsets 1, 2, 3, 4 and 5, respectively (Figs. 2–4).

The MTM power spectrum of the 405 kyr-calibrated Th series shows obvious spectral peaks with the periodicity of 410, 133, 100.2, 27, 21.3 and 18.3 kyr above the 99% CL; the periodicities of 39.5 and 22.5 kyr above the 95% CL; the periodicity of 37.9 kyr above the 90% CL (Fig. 7). These spectra agree well with those of the expected Late Cretaceous astronomical terms and therefore, support our cyclostratigraphic analysis results, and allow us to establish a "floating" ATS for the SK-2 borehole.

4.2 "Floating" ATS and durations of the stratigraphic formations

One of the main objectives of this study was to construct an ATS for the SK-2 borehole. However, because of the absence of fossils and direct radioisotope ages for this core, it is difficult to build an absolute time framework. Two oil shale layers developed in K_2n and K_2qn of the SK-1s and SK-2 boreholes are considered to be isochronous. Here we anchor the CA-ID-TIMS U–Pb age of 83.269 ± 0.044 Ma from the SK-1s borehole (Wang et al., 2016) to the depth of 1145 m in the SK-2 borehole, because both these levels correspond to the same bedded oil shale at the bottom of K_2n^2. Considering that a 405-kyr cycle was overlooked or counted twice, a ± 0.4 Myr uncertainty of cycle counting was suggested in our new ATS. A "floating" ATS of the SK-2 borehole was established from 77.62 Ma to 96.24 Ma with a total duration of 18.62 ± 0.4 Myr (Fig. 8). The constructed ATS indicates that the durations of the K_2n, K_2y, K_2qn and K_2q are ~6972.1, ~1832.2, ~5301.4 and ~4518.7 kyr, respectively. The astronomically calibrated boundary ages of contiguous stratigraphic members are obtained and shown in Fig. 8.

4.3 Comparison of the results between the SK-2 and SK-1s boreholes

Based on the "floating" ATS, the age of the other oil shale layer lies in the bottom of the K_2qn^1 was calculated

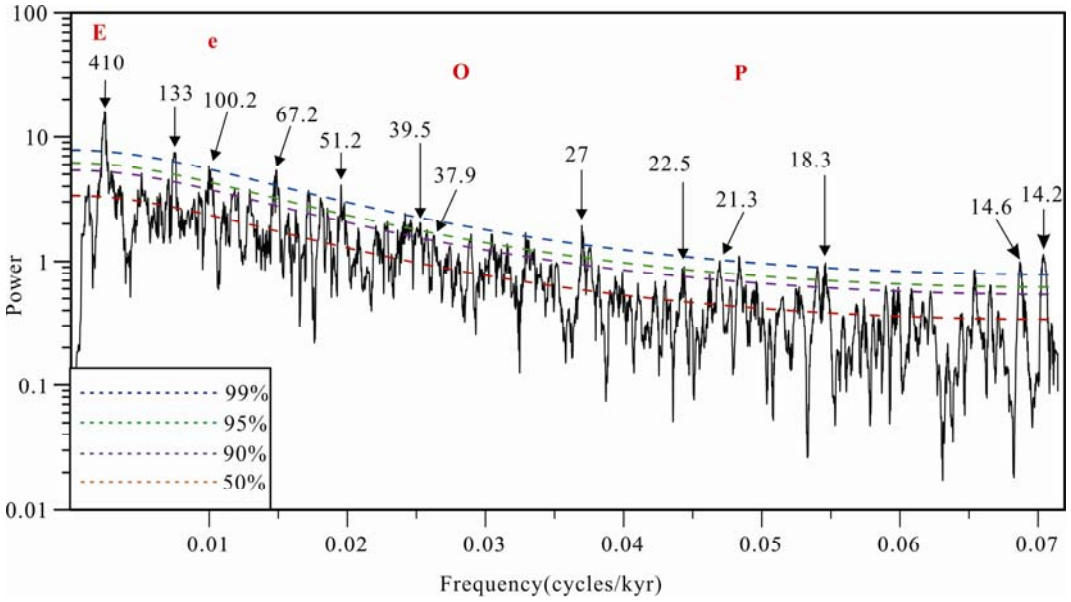

Fig. 7. 2π MTM power spectra of the 405 kyr-calibrated Th time series of the SK-2 borehole.
Frequency peaks are labeled in kyr. The red, purple, green and blue dashed lines represent the 50%, 90%, 95% and 99% CLs.

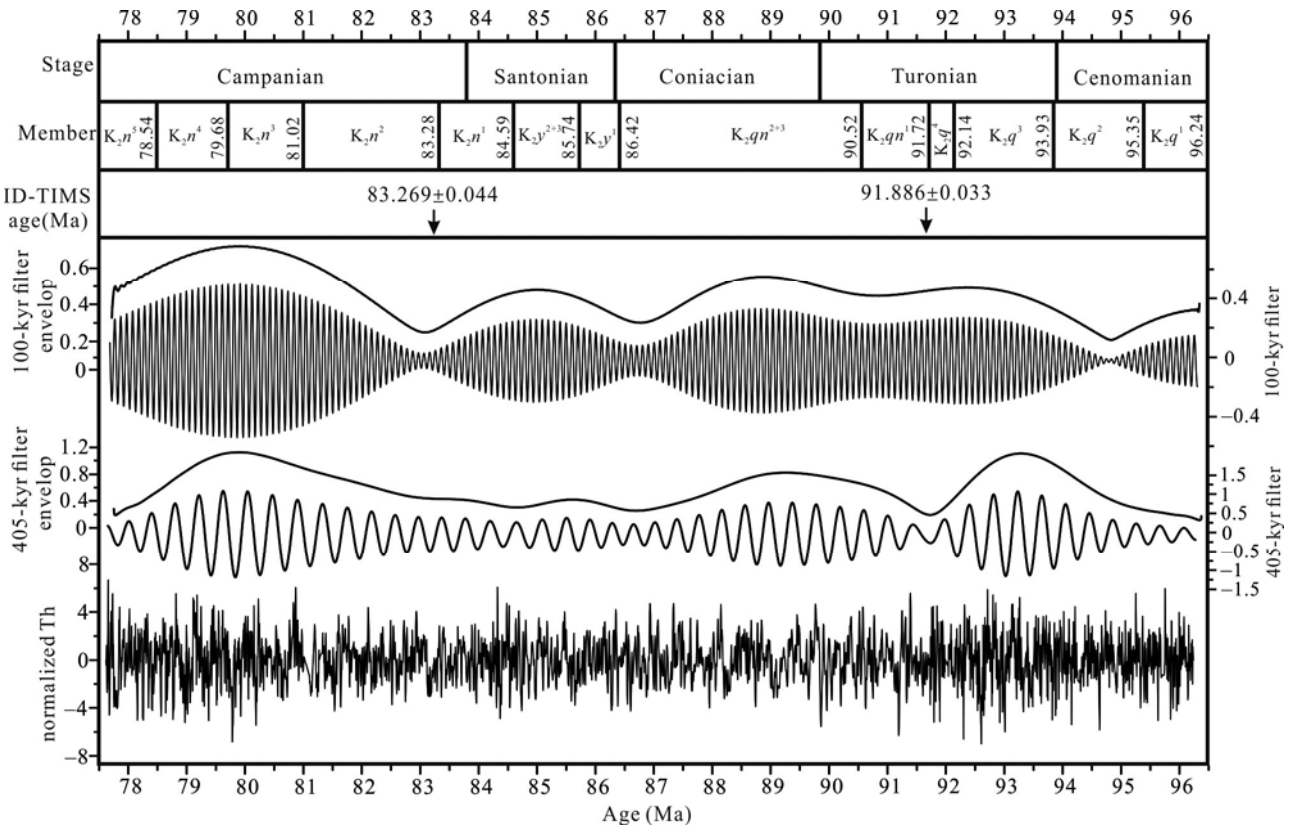

Fig. 8. Astrochronology age framework for the SK-2 borehole.
Shown from the top are stages with boundary ages, members with boundary ages, CA-ID-TIMS U–Pb ages from SK-1s core (Wang et al., 2016), the envelop of 100-kyr filter output, the extracted 100-kyr eccentricity cycles, the envelop of 405-kyr filter output, the extracted 405-kyr eccentricity cycles and the 405-kyr-turned Th logging data.

as 91.507 Ma, exhibiting a 0.379 Myr difference with the date of 91.886 ± 0.033 Ma (Wang et al., 2016) from the SK-1s borehole. Considering the potential uncertainties associated with the accuracy of the analyzed periodicity, an error within 1 long eccentricity cycle between the two ages should be incorporated. This result verifies the accuracy of our ATS, which provides new precise numerical ages for stratigraphic boundaries, biozones and geological events in the Songliao Basin (Fig. 8).

The cyclostratigraphic analysis and astronomical calibration of the SK-1s borehole were conducted by Wu et al. (2013), in which the U–Pb zircon TIMS age of 91.4 ± 0.6 Ma at the 1780 m depth obtained by He et al. (2012) was used as an anchor point. The strata in the study of Wu et al. (2013) were from K_2q^3 to K_2n^2, a little shorter than the sequence considered in the present study. The aim of both studies was to provide a precise time framework for the Upper Cretaceous succession in the Songliao Basin, so it is ponderable to compare the two. Because of the lack of an ATS for $K_2n^{3–5}$ and K_2q^{1+2} in the SK-1s core, the comparison only includes K_2n^{1+2}, K_2y and K_2qn.

The strata from K_2q to K_2n are well developed in both the SK-1s and SK-2 boreholes, but with different thicknesses (Table 1). The sedimentary deposits of the K_2y and K_2qn in the SK-1s borehole are thicker than those in the SK-2 borehole, whereas the K_2n^{1+2} in the SK-1s borehole is thinner than that in the SK-2 borehole. From analyses of the stratigraphic sequence and depositional environment of the Songliao Basin (Wang et al., 2007; Feng et al., 2010), the sedimentary facies and lithological associations of the two boreholes are generally similar. However, Fan et al. (2017) discovered that from K_2q^3 to K_2n^3, the depocenter migrated from the Qijia Sag to the Sanzhao Sag, which highlighted the migration of the deltaic lobe in a direction of SW–NW–NE. Thus, we infer that the migration of the depocenter may have been the conclusive factor resulting in the differences in bed thickness and SAR between the two boreholes.

For K_2qn, the duration of 5.361 Myr from the SK-1s borehole is well in consistent with that of 5.301 Myr from the SK-2 borehole, with a difference of 0.06 Myr. As a result, the average SAR of K_2qn exhibits just parallel trends with formation thickness: higher SAR values correspond to thicker sedimentary deposits in the SK-1s borehole than those in the SK-2 borehole (Table 1). However, the durations of K_2y indicate bias of ca. 0.459 Myr between the two boreholes. Wu et al. (2009) conducted an elaborate cyclostratigraphic analysis of K_2qn using GR logging data from 10 wells, and it demonstrated variable durations of K_2qn across the basin (1.09 Myr–5.20 Myr) and strong diachroneity of the lacustrine strata. Thus, it is reasonable that same member in different parts of the basin represent different durations. For K_2n^{1+2}, a greater than 2 Myr discrepancy of duration is present between the two boreholes. From the consistency of the durations between our ATS and the absolute radioisotopic

geochronology of Wang et al. (2016), we share the same perspective that the ATS of K_2n from the SK-1s borehole may have hypothesized an excessively large SAR, which led to a shorter duration.

5 Conclusions

Spectral analysis of Upper Cretaceous terrestrial strata of the SK-2 borehole shows significant astronomical signals with frequency components indicative of the long eccentricity, short eccentricity, obliquity and precession cycles, indicating that the sedimentation in the Songliao Basin of northeastern China was astronomically controlled. Synchronizing the oil shale from the SK-1s and SK-2 boreholes, a time scale for the period 77.62–96.24 Ma was established.

(1) The "floating" ATS identifies the total duration of the entire study section is 18.62 Myr, with the durations of K_2n, K_2y, K_2qn and K_2q being 6.972, 1.832, 5.301 and 4.519 Myr, respectively. Our ATS is basically in consistence with the U–Pb geochronology result from the SK-1s borehole, with an acceptable difference of 0.379 Myr.

(2) COCO analyses of the five subsets verify the existence of orbital signal in the Th logging series and reveal the change of SAR during the post-rift thermal subsidence stage as follows: K_2q has the highest SAR of 19.01 cm/kyr, and K_2n^{3-5} the second highest, because two subsidence fastigium occurred during deposition o f K_2q and K_2n. SAR values are consistently low for K_2qn, K_2y and K_2n^{1+2} because of the great lake transgression in K_2qn^1 and K_2n^{1+2}.

(3) Comparison of the ATS results between SK-1s and SK-2 shows that: for K_2qn, the durations of the two boreholes are in good agreement, with values of 5.361 Myr for the SK-1s borehole and 5.301 Myr for the SK-2 borehole; For K_2y, the duration indicates a bias of ca. 0.459 Myr between the two boreholes, which may result from the strong diachroneity of the lacustrine strata; For K_2n^{1+2}, a large discrepancy of duration exists between the two boreholes and it is likely that Wu et al. (2013) has hypothesized an excessively large SAR, which led to a shorter duration.

Acknowledgements

The logging data used in this study is provided by the ICDP SK-2 drilling project. The authors greatly appreciated the help from Jichuang Fang. This study was supported by the National Natural Science Foundation of China (41790451, 41925010, and 41688103), National Key R&D Program of China (2019YFC0605403) and the subject development project of RIPED (yjkt2019-3).

Manuscript received Nov. 29, 2019
accepted Jan. 13, 2020
associate EIC FEI Hongcai
edited by FEI Hongcai

Reference

Chamberlain, C.P., Wan, X.Q., Graham, S.A., Carroll, A.R., Doebbert, A.C., Sageman, B.B., Blisniuk, P., Kent-Corson, M.L., Wang, Z., and Wang, C.S., 2013. Stable isotopic evidence for climate and basin evolution of the Late Cretaceous Songliao Basin, China. Palaeogeography Palaeoclimatology Palaeoecology, 385: 106–124.

Deng, C.L., He, H.Y., Pan, Y.X., and Zhu, R.X., 2013. Chronology of the terrestrial Upper Cretaceous in northeast Asia. Palaeogeography Palaeoclimatology Palaeoecology, 385: 44–54.

Fan, Q., Fan, T.L., Tian, J.J., Sun M.H., and Li, S., 2017. Sequence stratigraphy and sedimentary evolution from the 4th member of Quantou Formation to the 3rd member of Nenjiang Formatin in Sifangtuozi area, Songliao Basin. Petroleum Geology & Experiment, 39(5): 593–602 (in Chinese with English abstract).

Feng, Z.Q., Jia, C.Z., Xie, X.N., Zhang, S., Feng, Z.H., and Cross, T.A., 2010. Tectonostratigraphic units and stratigraphic sequences of the nonmarine Songliao Basin, northeast China. Basin Research, 22(1): 79–95.

Fiet, N., Beaudoin, B., and Parize, O., 2001. Lithostratigraphic analysis of Milankovitch cyclicity in pelagic Albian deposits of central Italy: Implications for the duration of the stage and substages. Cretaceous Research, 22(3): 265–275.

Gao, R.Q., Zhang, Y., and Cui, T.C., 1994. Cretaceous Petroleum Bearing Strata in the Songliao Basin. Beijing: Petroleum Industry Press, 1–333 (in Chinese with English abstract).

Gao, Y., Ibarra, D.E., Wang, C.S., Caves, J.K., Chamberlain, C.P., Graham, S.A., and Wu, H.C., 2015. Mid-latitude terrestrial climate of East Asia linked to global climate in the Late Cretaceous. Geology, 43: 287–290.

Gao, Y., 2015. Paleoclimate evolution of the Songliao Basin in the Late Cretaceous: Evidences from the SK-1 Continental Scientific Drilling (Ph.D. thesis). Beijing: China University of Geoscience for Doctoral Degree, 1–99.

Grippo, A., 2003. Cyclostratigraphy and chronology of the Albian stage (Piobbico core, Italy) (Ph.D. thesis). Los Angeles: University of Southern California, 1–111.

He, H.Y., Deng, C.L., Wang, P.J., Pan, Y.X., and Zhu, R.X., 2012. Toward age determination of the termination of the Cretaceous Normal Superchron. Geochemistry Geophysics Geosystems, 13: Q02002. http://dx.doi.org/10.1029/2011GC003901.

Hu, J.F., Peng, P.A., Liu, M.Y., Xi, D.P., Song, J.Z., Wan, X.Q., and Wang, C.S., 2015. Seawater incursion events in a Cretaceous paleo-lake revealed by specific marine biological markers. Scientific Reports, 5: 9508.

Huang, Q.H., Zheng, Y.L., Yang, M.J., Li, X.J., Han, M.X., and Chen, C.R., 1999. On Cretaceous paleoclimate in the Songliao Basin. Acta Micropalaeontologica Sinica. 16(1): 95–103 (in Chinese with English abstract).

Huang, Y.J., Yang, G.S., Gu, J., Wang, P.K., Huang, Q.H., Feng, Z.H., and Feng, L.J., 2013. Marine incursion events in the Late Cretaceous Songliao Basin: Constraints from sulfur geochemistry records. Palaeogeography. Palaeoclimatology. Palaeoecology, 385: 152–161.

Huson, D., Galbrun, B., Laskar, J., Hinnov, L.A., Thibault, N., Gardin, S., and Locklair, R.E., 2011. Astronomical calibration of the Mastrichtian (Late Cretaceous). Earth and Planetary Science Letters, 305(3): 328–340.

Kodama, K.P., and Hinnov, L.A., 2015. Rock Magnetic Cyclostratigraphy. New Jersey: Wiley-Blackwell, 1–165.

Laskar, J., Robutel, P., Joutel, F., Gastineau, M., Correia, A.C.M., and Levrard, B., 2004. A long-term numerical solution for the insolation quantities of the Earth. Astronomy and Astrophysics, 428(1): 261–285.

Laskar, J., Gastineau, M., Delisle, J.B., Farrés, A., and Fienga, A., 2011. Strong chaos induced by close encounters with Ceres and Vesta. Astronomy and Astrophysics, 532: L4.

Li, C., Liu, S.F., and Bai, Y., 2014. Differentiation of anomalous Cretaceous post-rift subsidence in southern Songliao Basin. Geoscience, 28(6): 1213–1224 (in Chinese with English abstract).

Li, M.S., Kump, L.R., Hinnov, L.A., and Mann, M.E., 2018. Tracking variable sedimentation rates and astronomical forcing in Phanerozoic paleoclimate proxy series with

evolutionary correlation coefficients and hypothesis testing. Earth and Planetary Science Letters, 501: 165–179.
Locklair, R.E., and Sageman, B.B., 2008. Cyclostratigraphy of the Upper Cretaceous Niobrara Formation, Western Interior, U.S.A.: a Coniacian–Santonian orbital timescale. Earth and Planetary Science Letters, 269(3–4): 540–553.
Ma, C., Meyers, S.R., Sageman, B.B., Singer, B.S., and Jicha, B.R., 2014. Testing the astronomical time scale for oceanic anoxic event 2, and its extension into Cenomanian strata of the Western Interior Basin (USA). Geological Society of America Bulletin, 126(7–8): 974–989.
Meyers, S.R., 2014. Astrochron: An R Package for Astrochronology. Version 0.7. https:// cran.r-project.org/ package=astrochron.
Meyers, S.R., Siewert, S.E., Singer, B.S., Sageman, B.B., Condon, D.J., Obradovich, J.D., Jicha, B.R. and Sawyer, D.A., 2012. Intercalibration of radioisotopic and astrochronologic time scales for the Cenomanian-Turonian boundary interval, Western Interior Basin, USA. Geology, 40 (1): 7–10.
Olsen, P.E., and Kent, D.V., 1996. Milankovitch climate forcing in the tropics of Pangaea during the Late Triassic. Palaeogeography Palaeoclimatology Palaeoecology, 122(1–4): 1–26.
Olsen, P.E., and Kent, D.V., 1999. Long-period Milankovitch cycles from the Late Triassic and Early Jurassic of eastern North America and their implications for the calibration of the early Mesozoic time-scale and the long-term behaviour of the planets. Philosophical Transactions of the Royal Society. A: Mathematical, Physical and Engineering Sciences, 357(1757): 1761–1786.
Schnyder, J., Ruffell, A., Deconinck, J.F., and Baudin, F., 2006. Conjunctive use of spectral gamma-ray logs and clay mineralogy in defining late Jurassic-early Cretaceous palaeoclimate change (Dorset, UK). Palaeogeography Palaeoclimatology Palaeoecology, 229(4): 303–320.
Sha, J.G., 2007. Cretaceous stratigraphy of northeast China: non-marine and marine correlation. Cretaceous Research, 28(2): 146–170.
Thomson, D.J., 1982. Spectrum estimation and harmonic analysis. Proceeding of the IEEE, 70(9): 1055–1096.
Wan, X.Q., Zhao, J., Scott, R.W., Wang, P.J., Feng, Z.H., Huang, Q.H., and Xi, D.P., 2013. Late Cretaceous stratigraphy, Songliao Basin, NE China: SK1 cores. Palaeogeography Palaeoclimatology Palaeoecology, 385: 31–43.
Wang, C.S., Feng, Z.Q., Zhang, L.M., Huang, Y.J., Cao, K., Wang, P.J., and Zhao, B., 2013b. Cretaceous paleogeography and paleoclimate and the setting of SKI borehole sites in Songliao Basin, northeast China. Palaeogeography Palaeoclimatology Palaeoecology, 385: 17–30.
Wang, C.S., Scott, R.W., Wan, X.Q., Graham, S.A., Huang, Y.J., Wang, P.J., Wu, H.C., Dean, W.E., and Zhang, L.M., 2013a. Late Cretaceous climate changes recorded in Eastern Asian lacustrine deposits and North American Epieric sea strata. Earth-Science Reviews, 126: 275–299.
Wang, P.J., Xie, X.A., Mattern, F., Ren, Y.G., Zhu, D.F., and Sun, X.M., 2007. The Cretaceous Songliao Basin: Volcanogenic succession, sedimentary sequence and tectonic evolution, NE China. Acta Geologica Sinica (English Edition), 81(6): 1002–1011.
Wang, T.T., Ramezani, J., Wang, C.S., Wu, H.C., He, H.Y., and Bowring, S.A., 2016. High-precision U-Pb geochronologic constraints on the Late Cretaceous terrestrial cyclostratigraphy and geomagnetic polarity from the Songliao Basin Northeast China. Earth and Planetary Science Letters, 446: 37–44.
Wu, F.Y., Sun, D.Y., Li, H.M., and Wang, X.L., 2001. The nature of basement beneath the Songliao Basin in NE China: geochemical and isotopic constraints. Physics and Chemistry of the Earth, Part A: Solid Earth and Geodesy, 26(43718): 793–803.
Wu, H.C., Zhang, S.H., Hinnov, L.A., Jiang, G., Yang, T.S., Li, H.Y., Wan, X.Q., and Wang, C.S., 2014. Cyclostratigraphy and orbital tuning of the terrestrial upper Santonian–Lower Danian in Songliao Basin, northeastern China. Earth and Planetary Science Letters, 407: 82–95.
Wu, H.C., Zhang, S.H., Jiang, G.Q., and Huang, Q.H., 2009. The floating astronomical time scale for the terrestrial Late Cretaceous Qingshankou Formation from the Songliao Basin of Northeast China and its stratigraphic and paleoclimate implications. Earth and Planetary Science Letters, 278(3–4): 308–323.
Wu, H.C., Zhang, S.H., Jiang, G.Q., Hinnov, L.A., Yang, T.S., Li, H.Y., Wan, X.Q., and Wang, C.S., 2013. Astrochronology of the Early Turonian–Early Campanian terrestrial succession in the Songliao Basin, northeastern China and its implication for long-period behavior of the Solar System. Palaeogeography Palaeoclimatology Palaeoecology, 385: 55–70.
Zhao, J., 2013. Late Cretaceous palynology (spores, pollen, algae), climate, and lacustrine conditions in Songliao Basin. (Ph.D. thesis). Beijing: China University of Geoscience for Doctoral Degree, 1–115.
Zhu, Y.Y., Wang, W.S., Wu, X.M., Zhang, H.C., Xu, J., Yan, J., Cao, L.L., Ran, H.Q., and Zhang, J.C., 2018. Main technical innovations of Songke well No. 2 drilling project. China Geology, 2: 187–201.

About the first author

MA Xiaojuan, female, born in 1992 in Wenzhou City, Zhejiang Province; PhD Candidate; from China University of Geosciences, Beijing. She is now interested in the study on Cyclostratigraphy of Cretaceous. Email: 906364691@qq.com; phone: 15201018569.

About the corresponding author

WU Huaichun, male, born in 1977 in Nanping City, Fujian Province. PhD. Graduated from China University of Geosciences, Beijing. He is now interested in the Cyclostratigraphy and Magnetostratigraphy. Email: whcgeo @cugb.edu.cn; phone: 15110289060.